Summer 2021

Groundwater Flow and Transport at the Forest-Marsh Boundary: A Modeling Study

Sophia Chason Sanders

Groundwater flow and transport at the forest-marsh boundary: A modeling study

by

Sophia Chason Sanders

Bachelor of Science
University of Georgia, 2019

Submitted in Partial Fulfillment of the Requirements

For the Degree of Master of Science in

Geological Sciences

University of South Carolina

2021

Accepted by:

Alicia Wilson, Director of Thesis

Jay Pinckney, Reader

Steve Pennings, Reader

Tracey L. Weldon, Interim Vice Provost and Dean of the Graduate School

DEDICATION

To my Teta, Leila.

ACKNOWLEDGEMENTS

I would like to thank my advisor, Dr. Alicia Wilson as well as my committee, Dr. Steven Pennings and Dr. Jay Pinckney. I would also like to thank the Long-Term Ecological Research Georgia Coastal Ecosystems section (LTER GCE) for the use of their data and resources. Additionally, I would like to thank Dontrece Smith for field assistance at Sapelo Island. This material is based upon work supported by the National Science Foundation under Grant No. 1832178 to the Georgia Coastal Ecosystems LTER. Any opinions, findings, and conclusions or recommendations expressed in this material are those of the author(s) and do not necessarily reflect the views of the National Science Foundation.

ABSTRACT

The forest-marsh boundary, where tidally influenced salt marshes meet a forested upland, is hydrologically complex due to its multiple water inputs. Groundwater flow and salinity transport at this boundary are not well understood. In order to make predictions about salinity at this boundary as it responds to climatic factors, a two-dimensional model was built to simulate groundwater flow and solute transport at a salt marsh on Sapelo Island, Georgia. After calibration based on observed data from wells at the study site, the model can be used to identify patterns in groundwater movement and solute transport that may influence the vegetation and consequently the migration of the forest-marsh boundary. Additionally, the model is designed to be a first step toward identifying the impacts of press and pulse disturbances, such as sea level rise or drought, on the marsh.

TABLE OF CONTENTS

LIST OF TABLES

LIST OF FIGURES

CHAPTER 1

INTRODUCTION

Salt marshes are highly productive ecosystems with an active community of organisms and plants specific to transitional wetlands. Marshes perform a variety of ecosystem services including mitigation of flooding during storm events and carbon sequestration (Costanza et al. 1997). Given these valuable services, it is important to understand the processes that support salt marsh ecosystems.

A characteristic feature of salt marshes is the distinct zonation of marsh plants. Most common in the Southeastern United States is *Spartina alterniflora*, a perennial grass that covers a majority of the low and mid-marsh (Mendelssohn and Morris, 2000). As elevation increases away from the creek, *S. alterniflora* height typically decreases (Mendelssohn and Morris, 2000). As marsh elevation increases, *Salicornia virginica*, now referred to as *Sarcocornia sp*., occurs in the hypersaline zone (Pennings and Richards, 1998). *Batis maritima* occurs further inland in the hypersaline zone, followed directly by *Juncus roemarianus* (Figure 1.1; Pennings and Richards, 1998). At the marsh-upland boundary, *Juncus roemarianus* is dominant (Wiegert & Freeman, 1990).

The distinct zonation of marsh plants reflects specific tolerances of root zone saturation and salinity, as well as competition between species (Pennings and Callaway 1992, Pennings et al. 2005). These plant zones migrate over time in response to changes in abiotic factors such as climate and sea level rise. Long term, gradual disturbances are described as press disturbances, whereas short-term, rapid disturbances are described as

pulse disturbances. Long-term monitoring of vegetation migration in salt marshes has indicated that changes in the amount of plant cover and the type of plant dominating the marsh are linked to changes in precipitation (Figure 1.2).

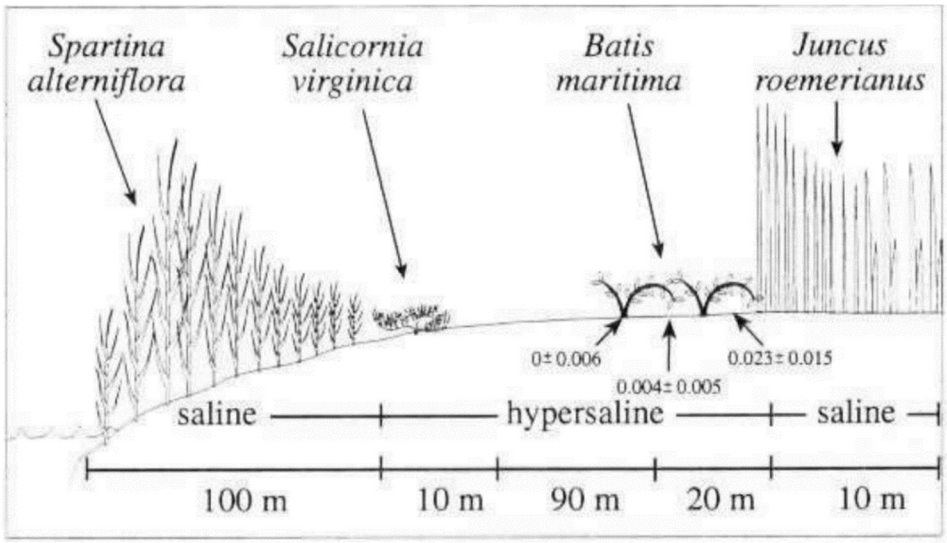

Figure 1.1. Salt marsh plant zonation on Sapelo Island, Georgia (Pennings and Richards, 1998).

Long-term records from the Georgia Coastal Ecosystems Long Term Ecological Research network (GCE LTER) on Sapelo Island, GA, showed that during a period of drought, *Sarcocornia sp*. and *Batis* cover increased while *Juncus* cover decreased. The lack of precipitation in this drought period would affect the salinity and the saturation of the root zone, thus allowing hypersaline-tolerant plants to perform well. However, it must be considered that these precipitation events were superimposed on gradual sea level rise over the 40-year monitoring period.

Groundwater flow in salt marshes is controlled by tides and precipitation. Salt marshes are characteristically tidally influenced, and groundwater flow patterns respond to this cycle as hydraulic head changes during the ebb and flow of the tides (Figure 1.3). Solute exchange across the sediment-water interface occurs in the highest volume when

the marsh is inundated and creek water infiltrates into the marsh surface (Wilson and Gardner, 2006). This carries solutes, notably salt, from the creek into the marsh. As the tide moves out, the marsh drains, transporting solutes downward and toward the creekbank.

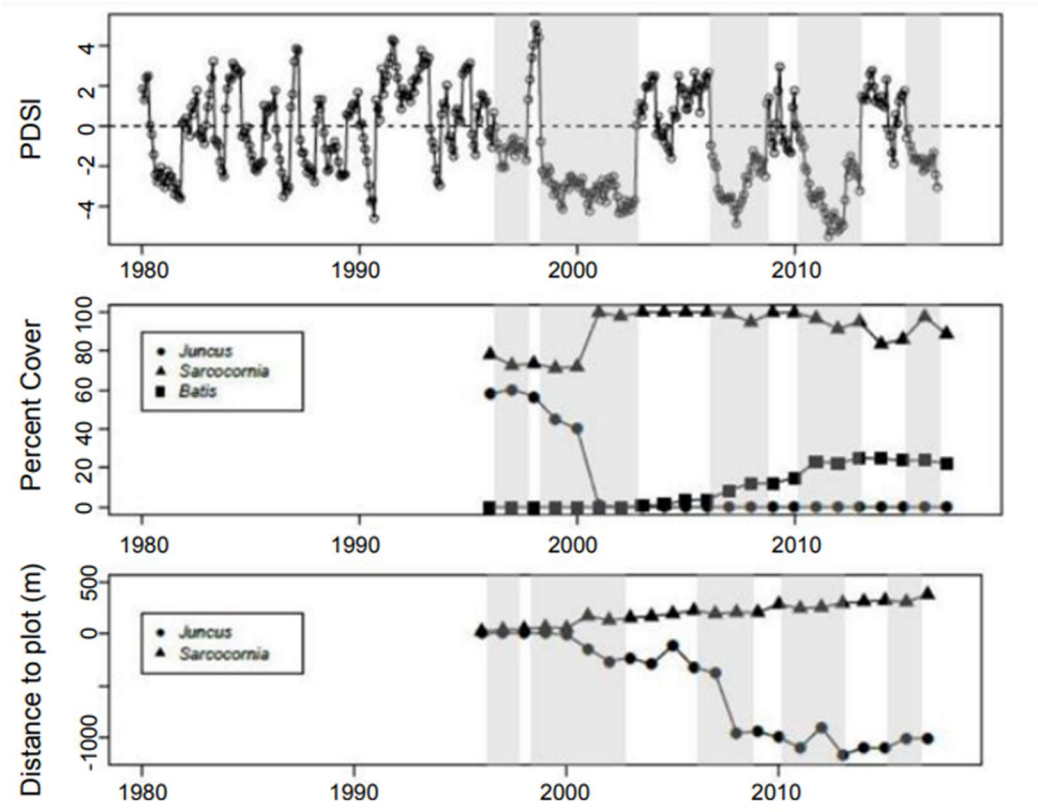

Figure 1.2. Marsh species response to drought(a) Palmer Drought Severity Index, (b) percent cover by vegetation averaged over 8 plots, (c) distance to plots over time measured from the middle of the plot to the edge of the plant zone. Negative values reflect plant retreat, positive values reflect plant advancement (Courtesy of S.C. Pennings)

Previous studies have been able to estimate salinity in the mid and low marsh with simple box models because net flow through the root zone is typically vertical (Miklesh and Meile, 2018; Morris, 1995). The main influences on salinity in the main marsh are infiltration of water into marsh sediments during inundation, drainage of this water into

deeper sediments during low tide, rainfall, and evapotranspiration (Miklesh and Meile, 2018). Salinity at the forest-marsh boundary is harder to predict because it is controlled by fresh groundwater inputs from the upland as well as the processes listed above for the mid and low marsh.

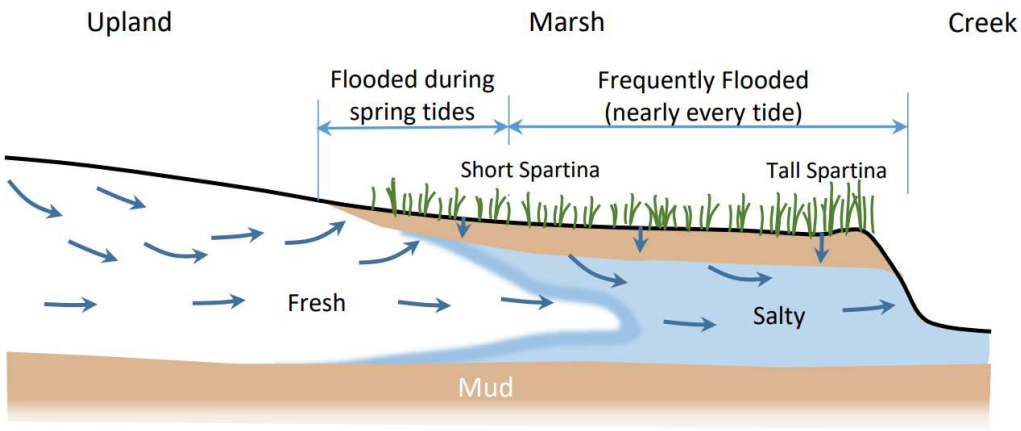

Figure 1.3. Conceptual model of groundwater flow through a marsh system over several tidal cycles (Courtesy of A.M. Wilson).

At the forest-marsh boundary, the hydrology is complicated by horizontal exchange. The forest-marsh boundary is in a zone of groundwater discharge, as the discharge from the upland and the inundated marsh intersect at this crux. When the marsh is draining, groundwater moves creekward from high hydraulic head to low hydraulic head, as is generally expected. However, when the marsh is inundated, the hydraulic head of the salt marsh can become higher than that of the forest-marsh boundary, resulting in flow towards this boundary from both the upland and the marsh. For this reason, one-dimensional models can not accurately estimate the salinity and aeration at this boundary, and a two-dimensional model is necessary.

Experiments have been done on Sapelo Island in which one meter of sheeting was installed vertically to prevent horizontal groundwater transport from the upland to the

marsh. This experiment did not cause changes in vegetation as hypothesized, nor did groundwater records indicate clear differences in salinity or hydraulic head compared to control plots. This raised questions about groundwater flow directions in the upper meter of the marsh. Modeling the groundwater flow in this system will provide insight into why this experiment failed to produce measurable results.

The goal of this study is to develop predictive models of the groundwater flow and salinity that can be used to explore flow patterns and major influences on salinity at the upland-marsh boundary. To this end, this project presents a process-based numerical model of groundwater movement in the marsh and at the forest-marsh boundary. The model is based on the salt marsh at Marsh Landing, Sapelo Island, Georgia, and is designed to allow us to draw connections between groundwater, salinity, aeration, and by extension, vegetation.

1.1 HYPOTHESES AND OBJECTIVES

The overarching hypothesis of this work is that the processes that influence groundwater flow and consequent changes in salinity at the forest-marsh boundary operate over a range of time scales and include flow components that cannot be captured by simple box models. Within this framework, we specifically hypothesize that:

a. H1

   At the forest-marsh boundary, temporal variations in salinity are more likely to be caused by variations in rainfall than variations in the tidal signal. This means that periods of drought or heavy rainfall are more likely to cause salinity to change than spring-neap

or seasonal variations in tidal signals. This contrasts with the low marsh, where changes in precipitation have limited effect.

b. H2

Changes in salinity in the high marsh reflect the expansion and contraction of the freshwater lens rather than direct infiltration of rainfall.

c. H3

Within the forest-marsh transition, the dominance of precipitation vs tidal fluctuations will vary with distance from the creek. Spatial variations in hydrology will correspond to plant zonation.

The objective of this study is to draw connections between tides, climate, the movement of groundwater in salt marshes, and the salinity at the forest-marsh boundary. This will provide a heightened understanding of the interconnectivity between tidal inputs, geology, and ecology of salt marshes. In order to identify these connections, a groundwater model will be built and calibrated to field data. By calibrating the model to observations at the field site, the model can be used to see how salinity is affected by press and pulse disturbances in a coastal salt marsh.

CHAPTER 2

METHODS

2.1 SITE DESCRIPTION

The salt marsh at Marsh Landing on Sapelo Island is an ideal field area for our study because it is the site of long-term ecological monitoring. Sapelo Island (31°21’57”N 81°03’08”W) is a barrier island in McIntosh County, Georgia and hosts many representative examples of southeastern salt marshes (Figure 2.1).

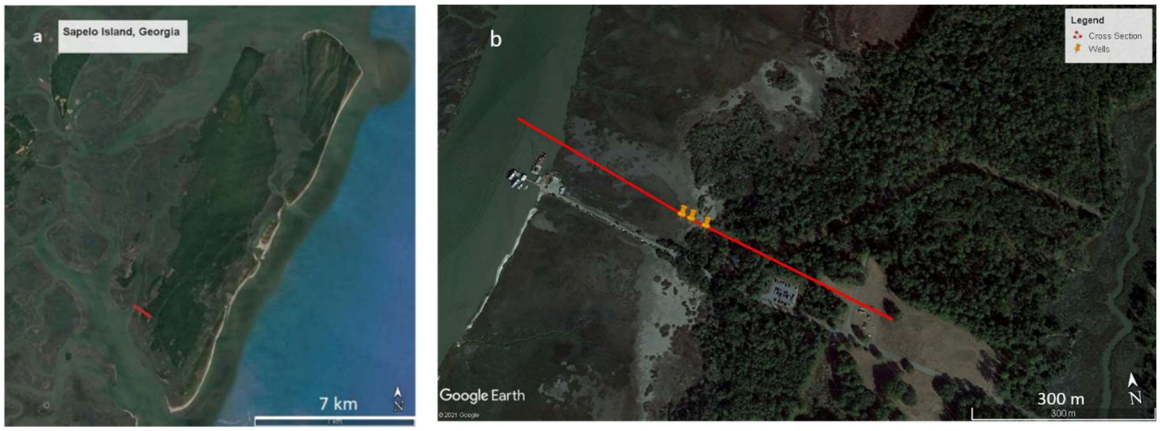

Figure 2.1. Study area. (a) Landsat image of Sapelo Island, Georgia. Red line indicates cross sectional length of model domain. (b) Marsh Landing, Sapelo Island, Georgia. Red line indicates the length of the model domain. Orange pins indicate location of monitoring wells.

The Marsh Landing study area is located along the Duplin River on the southwestern side of Sapelo Island. The area of interest is the marsh north of the ferry dock, which spans 350m from the river to the forest-marsh boundary. The plant monitoring sites lie in two transects that reach from the Duplin River to the forest-marsh

boundary (Figure 2.1b). The sites of interest in this study, where monitoring wells were installed, are within 100m of the forest-marsh boundary (Figure 2.2).

Figure 2.2. Well sites at Marsh Landing, Sapelo Island, Georgia.

2.2 WELL INSTALLATION

Monitoring wells were installed in the marsh in July of 2018 over a 50 m transect across the forest-marsh transition. The furthest creekward well is located about 439 m from the Duplin River, and the furthest landward is located 498 m from the river, at the forest-marsh transition. The wells increase in elevation from west to east (Table 2.1). Pressure and temperature data were collected at 15-minute intervals using CERA diver loggers. Hydraulic head was then calculated using the pressure data and logger elevations (Figure B.1). Salinity data was collected by hand sampling. Palmer Drought Severity Index (PDSI) values for Southeastern Georgia were obtained from the National Oceanic and Atmospheric Administration (NOAA).

Table 2.1. Coordinates and real time kinematic (RTK) elevations of logging wells. Based on NAD 83 datum.

Logger	Land surface elevation (m)	Logger elevation (cm)	Screen elevation (cm)	Latitude	Longitude
R2A	1.004	110.4	30.4	31°25'00.97916"N	81°17'34.99256"W
R2B	0.994	109.4	-20.6	31°25'00.95927"N	81°17'35.00630"W
R3A	1.07	117	47	31°25'00.64411"N	81°17'34.36862"W
R3B	1.047	114.7	-10.3	31°25'00.63045"N	81°17'34.38655"W
R4	1.449	154.9	-5.1	31°25'00.06366"N	81°17'33.42560"W

The stratigraphy of Marsh Landing was determined by hand augering at and between the wells. The stratigraphy data were then extrapolated to cover the entirety of the marsh cross section. This extrapolation was based on common stratigraphy in southeastern salt marshes (Gardner and Porter 2001, Weigert and Freeman 1990, Wilson et al. 2011).

2.3 MODEL CONSTRUCTION

A numerical model was used to simulate groundwater flow and transport, including water level and salinity at the forest-marsh boundary. The model was calibrated based on the hydraulic head and salinity data collected at the monitoring wells. The models were constructed following Evans and Wilson (2015), who used a version of SUTRA 2D3D (Voss & Provost, 2002) that has been modified to handle changing boundary conditions and other factors necessary for simulating tidal fluctuations (Wilson and Gardner, 2006).

The domain, a 2-D vertical cross section of the site, reaches from the apex of the upland to the middle of the Duplin River to place boundary conditions at natural hydraulic divides. The creekward boundary of the cross section was selected to be halfway through the Duplin instead of a creek in the marsh because the overall flow of the water is toward the Duplin, therefore making it a more appropriate flow divide than the small creek. The topography of the upper surface of the model was extracted by ArcMap using the ArcGIS digital elevation model (DEM) (Hladik and Alber, 2012). The DEM used was based on the NAVD88 datum. Some adjustments were made to the elevation in the model to deepen the Duplin and smooth out elevation anomalies created by trees. The lidar elevations used in the model had inconsistencies from the real time

kinematic (RTK) elevations of the wells of 20 cm at well R4, and elevation adjustments were made to the observed hydraulic heads, which were calculated using the RTK elevations, to correct for this elevation discrepancy. The RTK elevations were corrected to match the lidar because observed tidal inundation depths corroborated the lidar elevation data. The topographic high of the upland for Sapelo Island is about halfway across the island latitudinally. A specified flux boundary was imposed on the upper surface of the model, allowing rainfall or evapotranspiration (ET) when the node was exposed and allowing infiltration of tidal creek water when the node was inundated. The domain of the model is a 45 by 334 mesh. The mesh surrounding the sampling wells was made finer than that of the low marsh to ensure adequate resolution in the zone of interest while preserving processing speed (Figure 2.3).

In order to simulate the stratigraphy of Marsh Landing, a preprocessor was created to assign permeabilities and porosities to nodes within the mesh permeabilities and porosities based on the sediment types determined with hand augering (Appendix B). The preprocessor created an input file that contained the mesh with assigned permeabilities and porosities, observation nodes, and time step information. Other necessary input files contained tide data, precipitation, salinity, water density, and evapotranspiration as well as unsaturated flow parameters. The tidal data, obtained from the USGS Climate Station at Hudson Creek near Meridian, Georgia, was based on the NAVD88 datum. Using these, the model was run through different time periods.

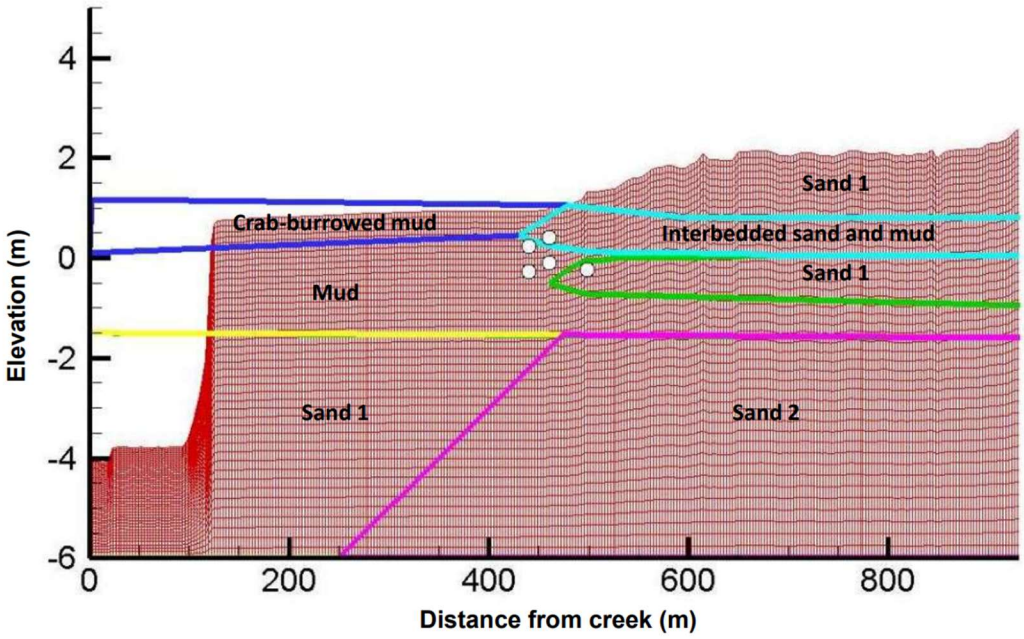

Figure 2.3. Model domain. Numerical mesh and polygons denoting areas of different sediment parameters. White points are locations of monitoring wells. Numbers refer to sediment types listed in Table 2.

Table 2.2. Descriptions of sediment types represented by polygons in Figure 6.

Sediment Number	Sediment Classification	Permeability	Minimum Permeability	Porosity
1	Sand	1.00E-09	1.00E-09	0.4
2	Crab-burrowed mud	1.00E-12	1.00E-12	0.72
3	Interbedded Sand and Mud	1.00E-09	1.00E-10	0.4
4	Mud	5.00E-13	5.00E-13	0.7
5	Sand	3.00E-09	3.00E-09	0.4

Hydraulic head observations and salinity measurements from the monitoring wells were used to calibrate the model. During calibration, the mud was further divided into a saturated mud and a crab-burrowed, higher permeability mud above it (Hughes et al. 1998; Xiao et al 2019). The crab burrowed mud layer had a permeability that was half an order of magnitude higher and was 2% more porous than the non-burrowed mud. Additionally, the crab burrowed mud was assigned unsaturated flow parameters, whereas the non-burrowed mud underlying it was assumed to be completely saturated and was not

assigned unsaturated flow parameters. The sand at the base of the sediment layers encompassed in our model was divided into two sections with slightly different permeabilities. The sand under the marsh had a permeability that was one third that of the sand under the upland, allowing more drainage below the upland (Figure 2.3). Unsaturated flow parameters were assigned for the crab-burrowed mud, sand, and interbedded sand and mud layer. The unsaturated flow parameters, particularly for the sand layer, were extremely important for the correct amount of filling and draining at each well.

An additional 3D version of the model was developed to test the possibility of radial flow, given the location of the transect near the southern end of the island. The z-dimension was changed from 1 to $z = 2\pi(L-x)$, where L is the total length of the transect, to create a wedge that allowed for more outward flow as the cross section approached the creek. Ultimately, the 2-dimensional model was determined to be a better fit and was used in this study. However, with more time and calibration, the 3D model could be improved to become a viable model of this system.

The model was run over two primary observation periods: June 1-23, 2020 and October 26, 2018 through December 31, 2020. The initial conditions for each of these runs were generated by running the model from January 2015 through the start date of the time period of interest. For example, the initial conditions for the June 1-23, 2020 run were created by running the model from January 1, 2015 - May 31, 2020 and the initial conditions for the October 2018 - December 2020 run were generated with a run from January 1, 2015 through October 25, 2018. The timing of the initial runs was chosen so that the initial conditions would be seasonally consistent with the times of interest. June

1-23, 2020 was used as a hydraulic head calibration run due to its representative spring-neap tidal cycle and precipitation events that were significant enough to cause a sharp increase in hydraulic head. October 26, 2018 - December 31, 2020 was chosen as a period of interest in order to compare simulated salinity with observed salinities, which were collected beginning October 26, 2018 through present.

CHAPTER 3

RESULTS

3.1 OBSERVATIONS

Three main sediment types were determined to be present in this system: a low-permeability mud, isotropic sand, and an interbedded layer of sand and silt. Hand augering revealed that the sediment at the Marsh Landing wells was generally silty sand between 0.30 m and one meter deep, underlain by a dense mud layer (Figure 3.1a). A conceptual cross section was created by extrapolating these data based on the common stratigraphy of southeastern salt marshes (Figure 3.1b).

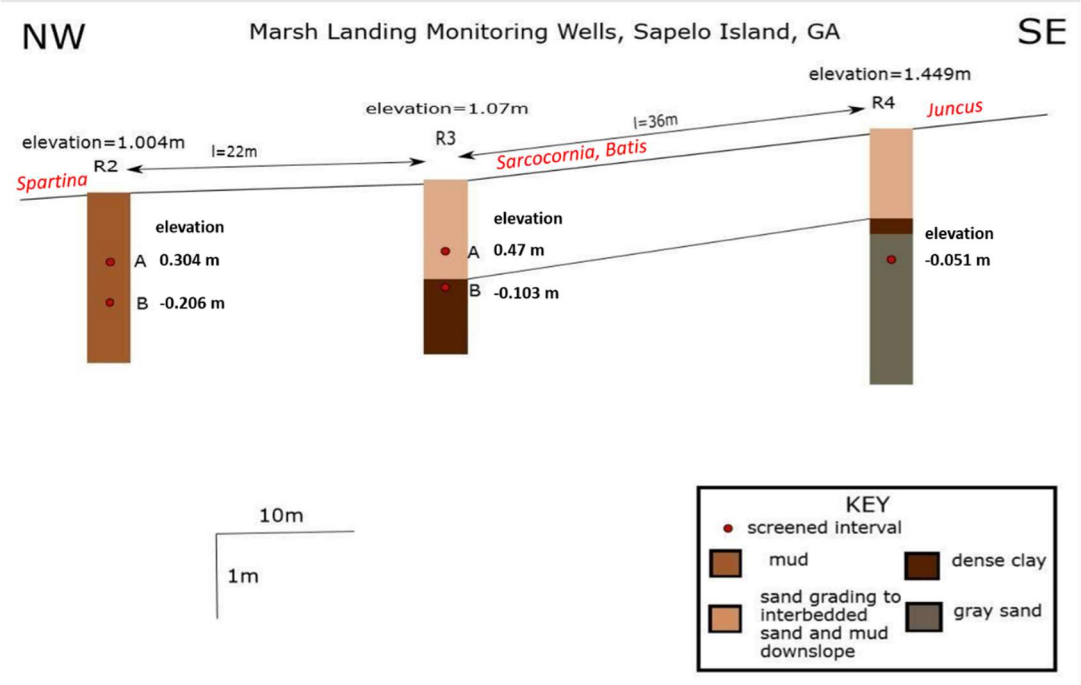

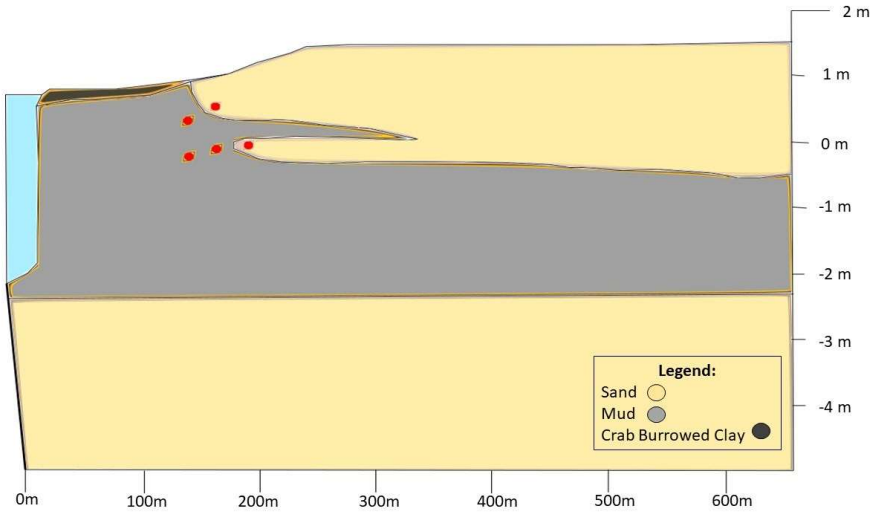

Figure 3.1 Cross sections of Marsh Landing. (a) Stratigraphy of the three wells at Marsh Landing, Sapelo Island, GA. Red dots indicate depths of screened well intervals.Listed elevations are based on real time kinematic (RTK) survey with NAD 83 datum. (b) Conceptual cross section of Marsh Landing, Sapelo Island, Georgia. Red points denote locations of the monitoring wells.

The hydraulic head in the wells increased and decreased in response to tidal fluctuations as well as precipitation (Figure 3.2). When the marsh was inundated during high tide, groundwater flow was generally upwards on the marsh platform (Figure A.2). When the marsh drained during low tide, flow is generally downward and creekward. Flow from the upland during low tides discharged at the forest-marsh boundary, whereas flow from the marsh discharged at the forest-marsh boundary when it was inundated (Figure 3.2). When the hydraulic gradient was positive, the flow was creekward from R4 to R3S. When the hydraulic gradient was negative, flow was landward toward R4 and the forest-marsh boundary. Overall, the general flow direction of the system was creekward. The salinity in the marsh overall remained relatively stable, with most of the wells reporting slightly fresher water in 2021 than 2018 (Figure 3.3). R2A was consistently the most saline, and R4 reported the lowest salinity.

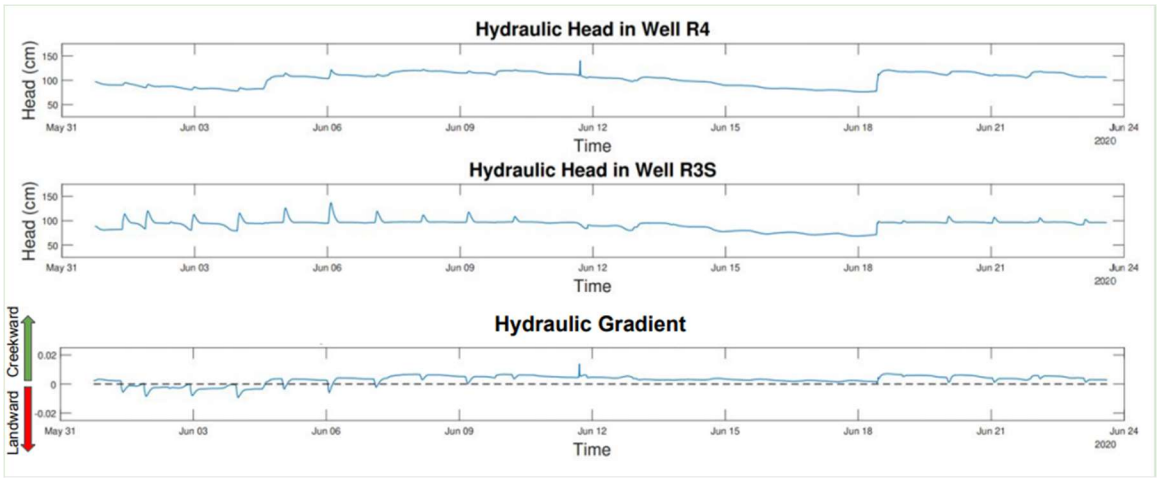

Figure 3.2. Hydraulic head at wells R4 and R3B, their head differences, and the hydraulic gradient between them over June 1-23, 2020.

The salinity at each well was negatively correlated with distance to the creek at most observation times. The exception to this was on June 5, 2019 and August 17, 2020, when the R3 well salinities were the same or greater than those of the R2B well. The most salinity measurements were obtained in spring and early summer of 2019 and 2020, and less data were recorded in the fall and winter seasons of 2019 and 2020. Salinity in most of the wells peaked June 5, 2019 and May 29, 2020. Wells R3A and R3B peaked later than the other wells in 2020, on August 17, 2020. These data indicate that salinity in the spring and summer months generally increases gradually and peaks in the late spring. These salinity observations do not provide enough data to identify patterns in fall and winter (Figure 3.3).

Records of precipitation and the PDSI revealed significant variations over the observation period. Throughout 2018, precipitation increased overall to peak at 127 mm of daily total precipitation on December 2, 2018. 2018 had a mean daily precipitation of 3.79 mm. NOAA recorded drought conditions with a PDSI value of -2 to -2.99 (moderate drought) in spring 2018, and May, July, August, and November 2018 (Figure 3.4).

NOAA recorded particularly moist conditions, with a PDSI value of +2.00 to +2.99 in December 2018 (Figure 3.4). 2019 was a drier year. Precipitation was fairly stable over the course of the year, with an overall increase in precipitation in November and a peak of 100 mm on December 22, 2019. The mean daily precipitation in 2019 was 2.84 mm. NOAA reported a PDSI value of -3 to -3.99 (severe drought) in September and October 2019. 2020 was wetter than either of the previous years. Frequent rain events were reported from mid-June through mid-August (Figure 3.4).

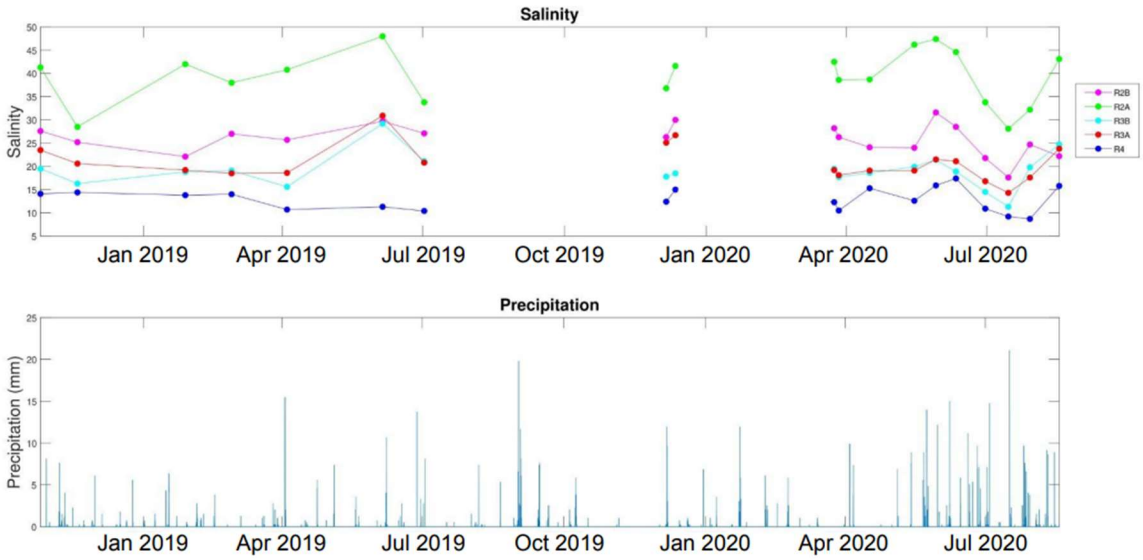

Figure 3.3. Observed salinities collected at Marsh Landing wells from late 2018 to spring 2021 versus the precipitation for the same time period.

3.2 MODEL CALIBRATION

Using the mesh, adjusted with sediment parameters, the model was calibrated to match observed data from May 31, 2020 at 6:55 PM to June 23, 2020 at 6:55 PM. This time frame was chosen because it was relatively representative of the tidal cycling that occurs in this system. June had a relatively high spring tide, and a neap tide began around halfway through the chosen time frame. This allowed us to ensure our model both filled

and drained appropriately during tidal cycles. Additionally, June had precipitation events that could be traced directly to increases in the hydraulic head. Particularly, a precipitation event on June 18 is directly reflected in the hydraulic head of the observed data (Figure 3.5). The peaks of the modeled data lined up precisely with the peaks of the observed data, which confirmed the correct alignment of the modeled time and observed time.

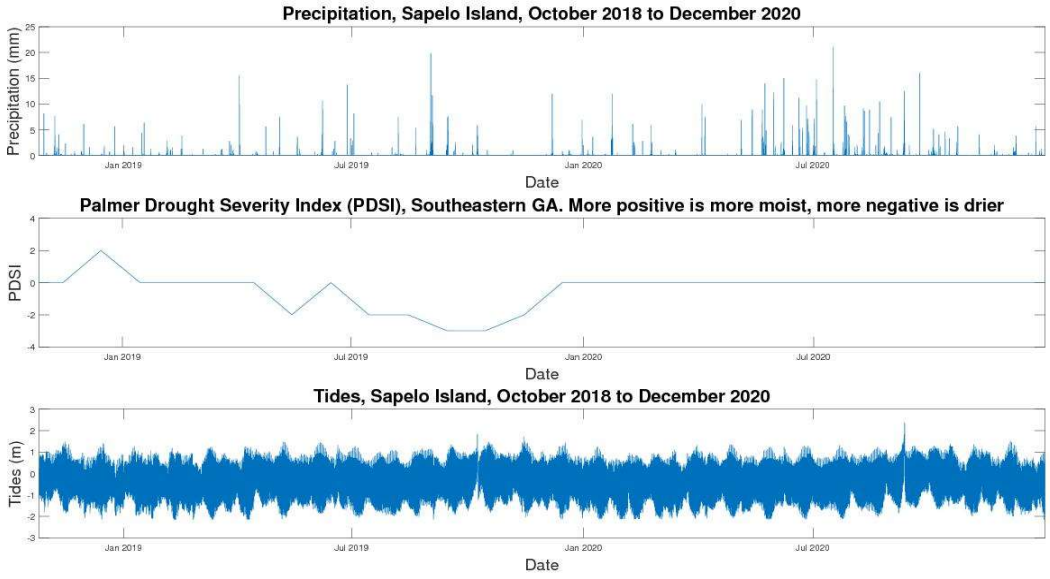

Figure 3.4. Tides and rainfall from October 26, 2018 – December 31, 2020.

The 3D version of the model allowed for too much drainage, and therefore was not used. The modeled hydraulic head in the 3D version immediately fell from initial conditions to between 50 and 65 cm, and remained flat for the remainder of the modeled time frame. None of the observed patterns were replicated by the 3D version of the model.

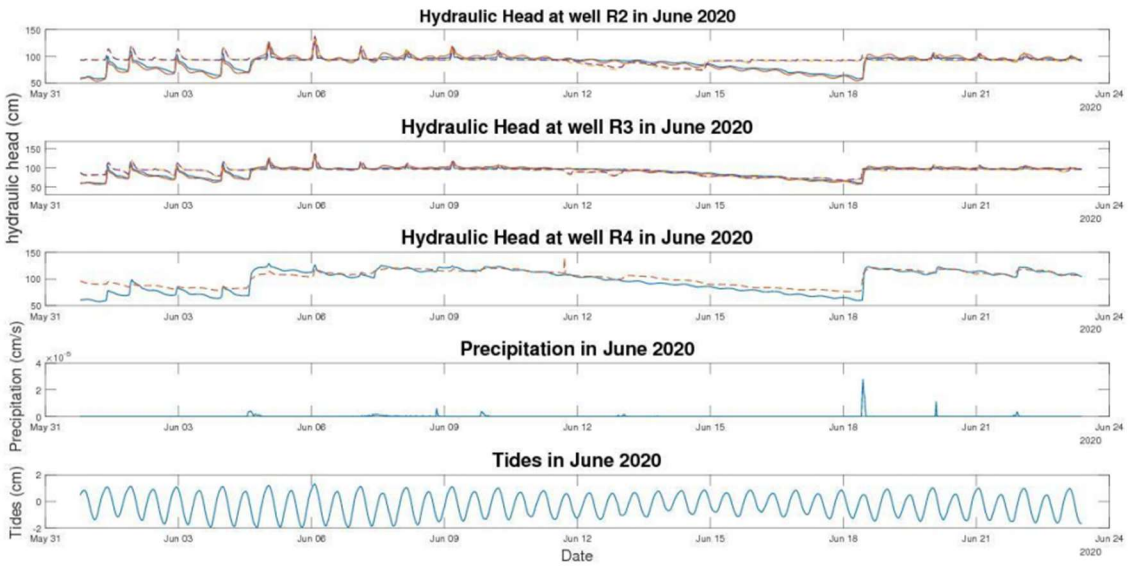

Figure 3.5. Modeled (solid) vs observed (dashed) hydraulic heads at the Marsh Landing monitoring wells during the calibration period, June 2020.

The modeled hydraulic head data and observed head data had an r^2 value of 0.50 and a root mean squared error (RMSE) of 11.26 cm. The R3 wells and well R4 shared similar observed drainage patterns, while R2 was different. While R3 and R4 wells drained from June 12 to June 18, the R2 wells only drained from June 12 to June 15. The worst fit was the R2 wells, as replicating the observed drainage timing for the upland wells and R2 was difficult. The conditions that caused drainage in the wells, primarily permeability and the unsaturated flow parameters of the sand, caused modeled drainage patterns in all three wells to drain from June 12 to June 18. The worst fit for all of the wells occurred in the first five days of the run, from June 1 through June 5. A period of excessive drainage occurred during this period, indicating that the initial conditions used for this run could be improved. Likely, the hydraulic head in the initial conditions is not high enough. From June 6, 2020 through the end of the month, the modeled hydraulic heads were a reasonably good fit to the observed hydraulic heads. The best fit was the

modeled R4 hydraulic head values, with an r-squared value of 0.89 and a root mean square error of 9.31 cm (Table A.3).

3.3 MODEL RESULTS

Simulated hydraulic head increased when the marsh was inundated, and the model showed overall upward flow during these periods of inundation, consistent with observed data. The hydraulic head decreased when the marsh drained, accompanied by net downward and creekward flow, again consistent with observed data (Figure 3.6).

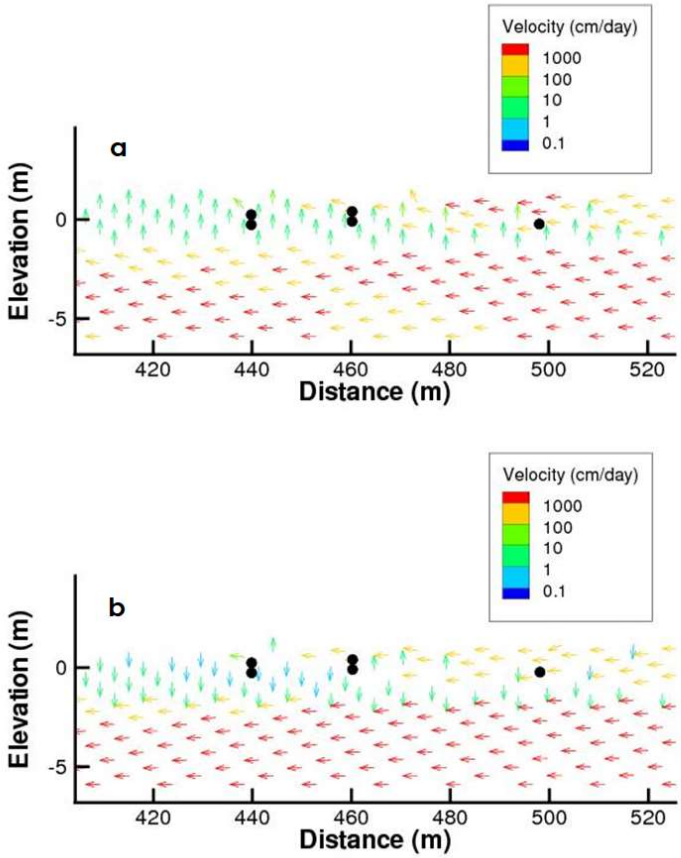

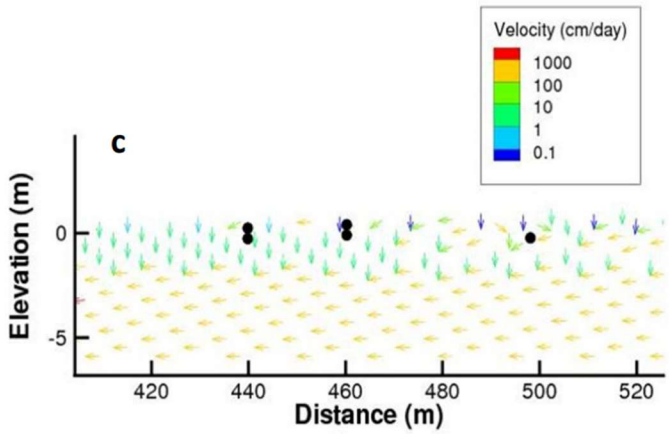

Figure 3.6. Flow directions at the forest marsh boundary during (a) high tide, (b) low tide, and (c) whole system drainage. Black points indicate well locations.

As expected, the marsh-upland boundary is an area of complex hydrology: precipitation from the upland seeped into this boundary area and groundwater flowed from the marsh toward the forest-marsh boundary when the marsh was inundated at high tide. At the forest-marsh boundary, seepage occurred from the upland. Flow directions at the forest-marsh boundary were generally upward and towards the exact point where the marsh begins to increase in elevation to become the upland. Flow in the uppermost layer of the marsh was overall horizontal, but upward diagonal flow directions at high velocities occurred during periods of upland seepage into the forest-marsh boundary (Figure 3.6b). From the marsh, water flowed upward and landward during times of inundation (Figure 3.6a). On larger time scales, the seepage zone at the forest-marsh transition moved on the spring-neap cycle and seasonally. Generally, flow directions indicated that the freshwater-salt water interface was between 450 m and 500 m from the creek. During spring tides, the zone moved landward to about 470 m from the creek. During neap tides, the zone moved creekward to about 450 m. This is consistent with the

findings of Wilson et al., 2015. On seasonal scales, the freshwater-salt water transition moved landward in the fall and remained there through the winter. During fall and winter in both 2019 and 2020, the seepage occurred at about 485 m from the creek. In the spring, the boundary moved back creekward to 460 m from the creek.

The saturation of the marsh seemed primarily responsive to pulse disturbances, with saturation in the marsh and upland being primarily driven by tidal cycling and precipitation, respectively. The simulated saturation increased during high tide and decreased during low tide, as expected. During low tides, saturation of the marsh at the creek bank decreased (Figure 3.7). Saturation in the marsh and upland was particularly high about once a month, indicating that it was responding to a spring tide. Conversely, during neap tides, the whole system was overall less saturated. While the marsh was almost completely saturated in most time steps, the upland had a much more prominent unsaturated zone ranging in thickness from 0.25 to 1.5 m. The upland and marsh almost seem disconnected with one another, as the unsaturated portion of the crab burrow layer rarely is contiguous with the unsaturated upland. Generally, the unsaturated zone was in the sandy upland, and all of the domain below this area remained saturated except during low tides. Additionally, the modeled saturation in the upland reflected the infiltration of precipitation (Figure 3.8). Following a precipitation event, such as on June 5, 2020, bands of saturation percolated through the unsaturated zone as rainfall infiltrated.

Salinity patterns produced by the model were lower than observed values but reflect expected patterns (Figure 3.9). The simulated salinity values reflected the patterns from the observed salinities reasonably well, with a peak in the late spring and a decrease through the summer. One disparity between the modeled and observed salinity values

occurred in July 2020, when the simulated salinities indicated an extra peak in salinity that the observed data did not reflect. Additionally, the simulated salinities were overall lower in 2020 than in 2019, which was inconsistent with the observed data. In observed and simulated data, salinity was higher at the marsh, and the upland was primarily fresh. Additionally, salinity was higher in the uppermost elevations of the marsh, and below the marsh mud was relatively fresh as solutes are not carried easily through the marsh mud. Simulated salinity did not respond much to spring-neap tide cycles but did exhibit seasonal patterns. Salinity in the marsh was higher during the summer, but salinity spread higher into the upland in the winter (Figure 3.10). Individual precipitation events did not affect modeled salinity much, and salinity would recover from rainfall events within one week of the event.

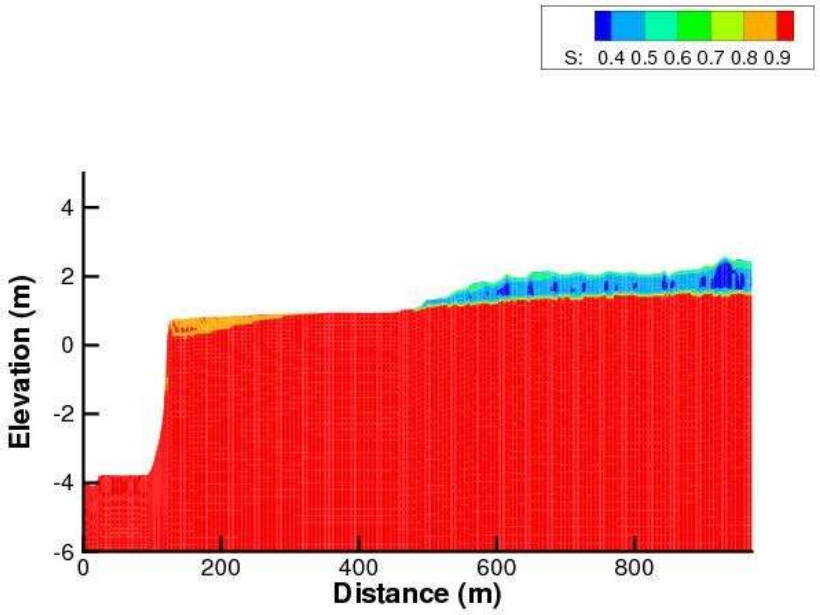

Figure 3.7. Modeled saturation of the marsh during a period of drainage.

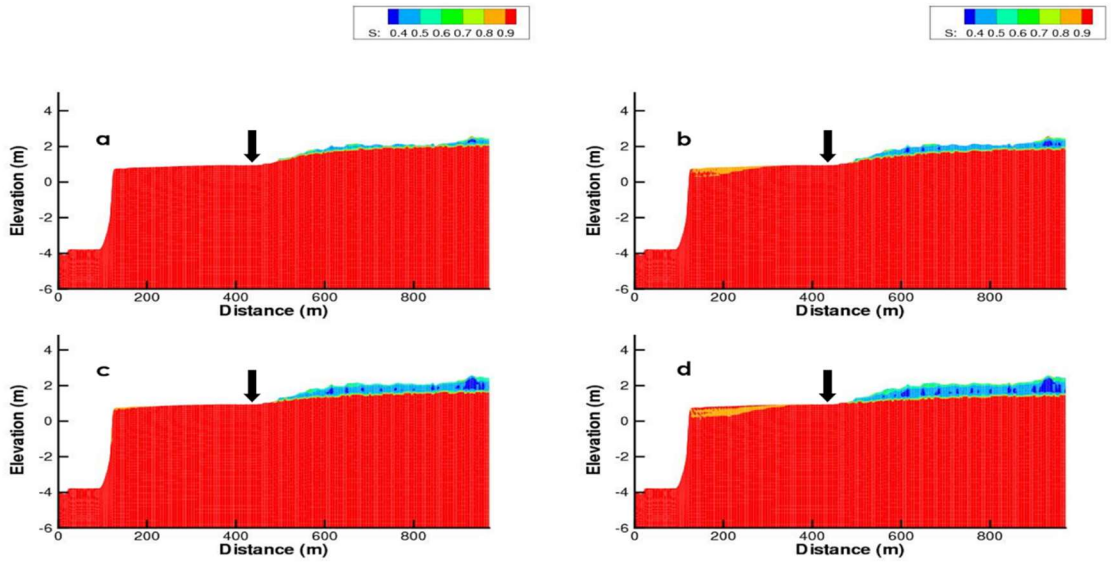

Figure 3.8. Saturation over a 48-hour period following a precipitation event on June 5. (a) 0 hours, low tide (b) 12 hours, low tide (c) 30 hours, high tide (d) 48 hours, low tide. Black arrows indicate location of the forest-marsh boundary.

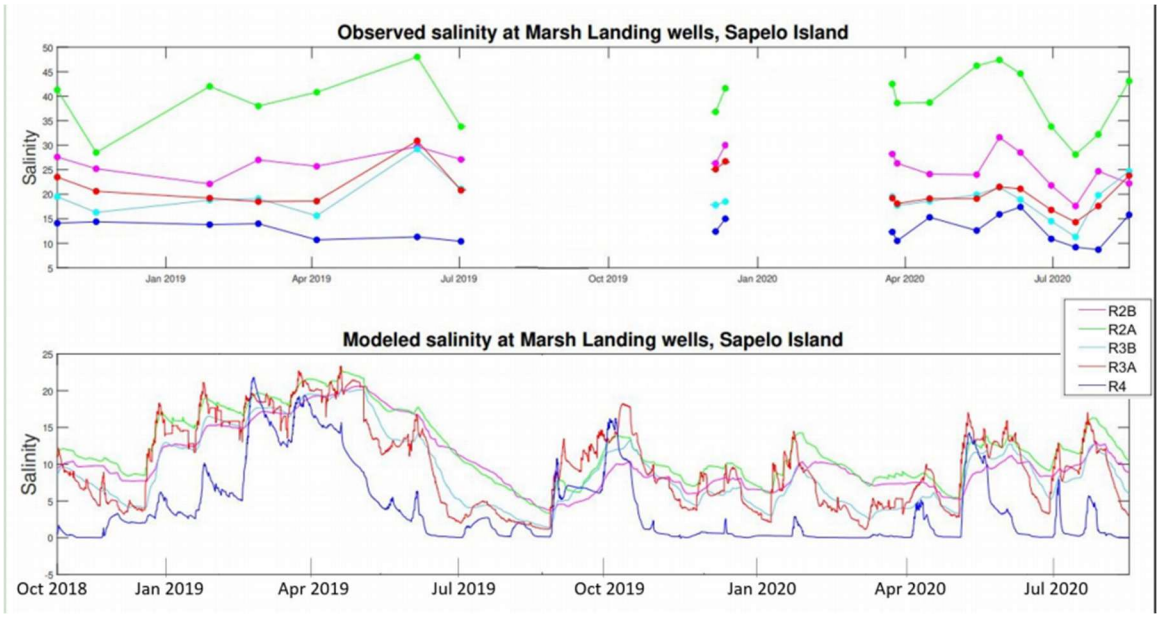

Figure 3.9. Observed versus modeled salinity at the Marsh Landing wells. Precipitation, drought, and tidal records for this period of time in Figure 10.

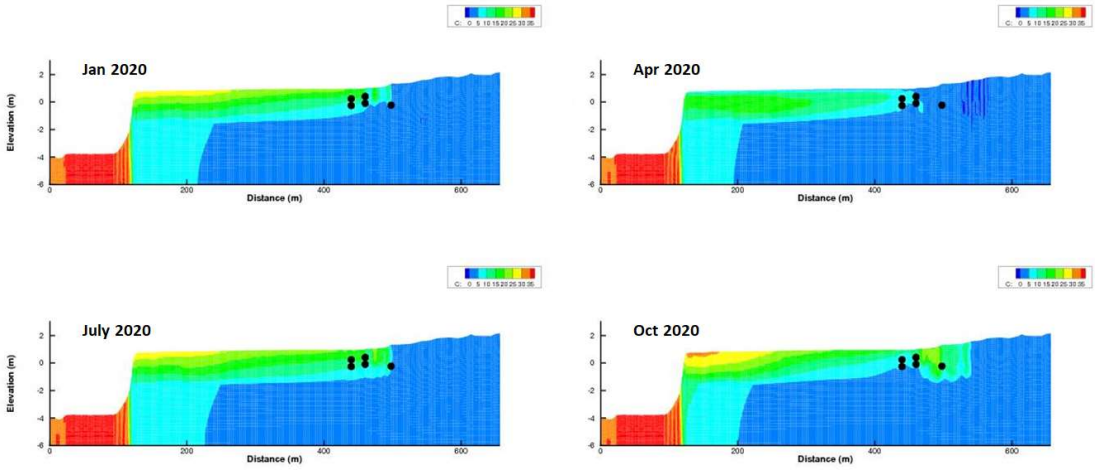

Figure 3.10. Modeled salinity values seasonally in 2020.

CHAPTER 4

DISCUSSION

Salinity in the model domain was primarily affected by seasonal variation. In winters, the fresh water-salt water interface in the models generally reached its furthest extent toward the upland (Figure 3.10). In fall, modeled salinity migrated toward the upland, and in spring, migrated toward the marsh. This is because mean sea level increased in the fall, allowing for more salt to be distributed to the upland. This increased salinity was not immediately flushed out by the freshwater flow in the upland, and salinity remained high in the upland through winter before decreasing in the spring. Overall, in summer, modeled salinity in the upland was low, but marsh salinity was higher than other seasons. In summer, increased evapotranspiration concentrated salt on the often-inundated marsh platform.

In the marsh, salinity was controlled by tidal inputs, and did not respond to precipitation. In the forest-marsh transition zone, salinity was affected by seasonal tidal variations and long-period variations in precipitation. In times of drought, such as fall 2019, the marsh platform was particularly salty, although the location of the fresh water-salt water interface did not seem to be affected. This disturbance did not last long, and the model returned to normal seasonal patterns by the end of the fall season. Salinity was primarily affected by the expansion and contraction of the freshwater lens rather than infiltration of precipitation from individual rainfall events. A drought of two months failed to generate lasting changes in salinity (Figure 4.1). For example, winter 2019,

directly following drought conditions, the salinity in the upland matched the salinity from the following winter closely, despite 2020 being a much wetter year overall. While salinity was not affected by individual precipitation events, it did seem to decrease during a rainy season such as summer 2020 (Figure 3.9).

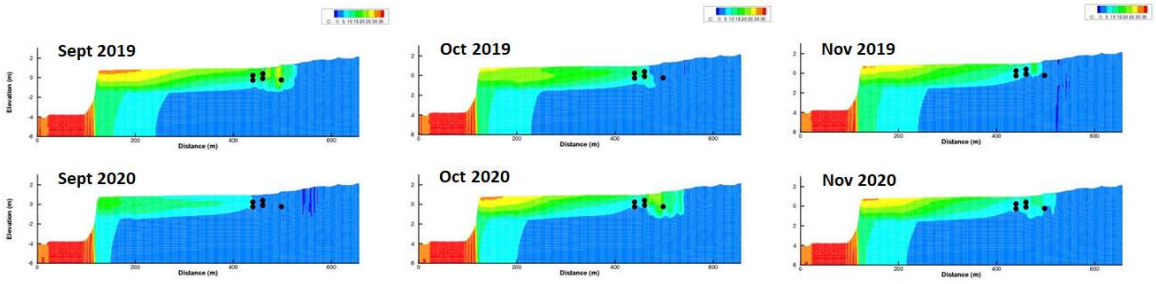

Figure 4.1. Modeled salinity through a period of severe drought in 2019 versus normal conditions in 2020.

Our 2D model suggests that the upland and marsh are hydrologically different systems connected to one another. While box models that do not consider discharge from the upland system have not worked, our results suggest that a box model connected to a 1D model may be able to represent this system. The 1D model is representative of the upland system, and when connected to a box model, would represent the forest-marsh boundary by inputting fresh groundwater into the box model representing the marsh platform. Our results also show, however, that the location of groundwater inputs from the upland into the marsh system is strongly influenced by stratigraphy. Thus, a paired 1D and box model has the potential to generate reasonable estimates of salinity at the forest-marsh transition, but local variations in stratigraphy may introduce errors.

During model construction and calibration, it became clear that models of groundwater flow through marshes depend heavily on accurate knowledge of

stratigraphy, unsaturated flow parameters, and elevation. Stratigraphic changes of a half a meter in depth or less caused the drainage patterns produced by the model to vary significantly. Consistency of the elevations of the water level from tidal inputs and land surface elevation is important for the correct general hydraulic head ranges because it was a critical control on when each site became inundated, though it had less of an effect on the drainage patterns at each well. Unsaturated flow parameters, particularly of the sand layer, also were extremely important for accurate amounts of drainage and filling at each well site. In order to build an accurate model of the salt marsh system we recommend testing elevation data against tidal inundation depths, determining unsaturated flow parameters from cores from the study site, and collection of stratigraphy in a wider and deeper area than was collected for this study.

The forest-marsh boundary can be identified by freshwater discharge through the root zone from the upland in addition to saltwater seepage from the marsh during high tides. Landward flow from the marsh is generally lower velocity than the upland seepage, and only occurs during marsh inundation at high tide. Flow directions at the forest-marsh boundary should generally be upward and towards the hinge point where the marsh begins to increase in elevation to become the upland. Modeling the forest-marsh boundary could be used to make predictions about how the hydrology of the forest-marsh boundary is affected as sea level rise continues to become a heightened threat. Additionally, patterns identified in these models can be feasibly applied to other Southeastern US salt marshes, as salt marshes in this region are similar in ecology and hydrology.

CHAPTER 5

CONCLUSIONS

In this study, a process-based 2D model was used to track groundwater flow and salinity at a southeastern US salt marsh. The salinity in the forest-marsh transition zone is reflective of the movement of the fresh water-salt water boundary. The fresh water-salt water boundary is moved by two separate systems: the upland system, which is affected by rainfall, and the marsh system, which is primarily affected by tides. Salinity at this boundary responds to longer pulse disturbances rather than daily tidal fluctuations or individual precipitation events. Although we hypothesized that the location of the fresh water-salt water boundary would be controlled by rainfall patterns rather than tides, we found that it was affected by a combination of seasonal variations in mean water level and long-scale weather changes.

The goal of this study was to trace the salinity in the marsh through seasonal variation and rainfall events as well as to assess whether a model of this system could be made with less complexity. The 2D model showed that the fresh water-salt water interface was controlled by the size of the freshwater lens. This supports the idea that a coupled 1D model to represent the upland with a box model to represent the marsh could model salinity reasonably well.

As southeastern salt marshes share many similarities both hydrologically and ecologically, this model can be applied to many study sites to track hydrologic changes through time. As sea level rise becomes a growing concern, insight into how it affects salt

marsh ecosystems is becoming critically important. The application of this model to many southeastern salt marsh sites will be useful in recognizing hydrologic patterns and their relationship to sea level rise and ecological changes.

WORKS CITED

Costanza, R. d'Arge, R., de Groot, R., Farber, S., Grasso, M., Hannon, B., Limburg, K., Naeem, S., O'Neill, R.V., Paruelo, J., Raskin, R.G., Sutton, P., van den Belt, M. 1997. The value of the world's ecosystem services and natural capital. *Nature* 387: 253-260.

Gardner, L.R. & Porter, D.E. 2001. Stratigraphy and geologic history of a southeastern salt marsh basin, North Inlet, South Carolina, USA. *Wetlands Ecology and Management* 9:371-385.

Hladik, C., Alber, M. 2012. Accuracy assessment and correction of a LIDAR-derived salt marsh digital elevation model. *Remote Sensing of Environment* 121: 224-235.

Hughes, C.E., Binning, P., Willgoose, G.R. 1998. *Characterisation of the hydrology of an estuarine wetland*. Journal of Hydrology 211: 34-49.

Mendelssohn, I. A. & Morris, J. T. 2002. Eco-Physiological Controls on the Productivity of Spartina Alterniflora Loisel. in *Concepts and Controversies in Tidal Marsh Ecology* (eds. Weinstein, M. P. & Kreeger, D. A.) 59–80

Milkesh, D., Meile, C. 2018. Porewater salinity in a southeastern salt marsh: Controls and interannual variation. *PeerJ* 6:e5911

Morris, J.T. 1995. The mass balance of salt and water in intertidal sediments: Results from North Inlet, South Carolina. *Estuaries* 18, 556–567

Pennings, S. 2020. High Marsh Update. Presented at Long Term Ecological Research Georgia Coastal Ecosystems annual conference.

Pennings, S. C. & Callaway, R. M. 1992. Salt Marsh Plant Zonation: The Relative Importance of Competition and Physical Factors. *Ecology* **73**, 681–690.

Pennings, S.C., Grant, M.B., Bertness, M.D. 2005. Plant zonation in low-latitude salt marshes: Disentangling the roles of flooding, salinity, and competition. *Journal of Ecology* **93(1):** 159-167.

Pennings, S.C., Richards, C.L. 1998. Effects of wrack burial in salt-stressed habitats: *Batis maritima* in a southwest Atlantic salt marsh. *Ecography* 21: 630-638.

Voss, C. I., and Provost, A.M. 2002., SUTRA, A model for saturated-unsaturated variable-density ground-water flow with solute or energy transport, U.S. Geological Survey Water-Resources Investigations Report 02-4231, 250 p.

Wiegert, R.G. & Freeman, B.J. 1990. *Tidal Salt Marshes of the Southeast Atlantic Coast: a Community Profile*. U.S. Department of the Interior, Fish and Wildlife Service, Washington, DC.

Wilson, A. M., Evans, T., Moore, W., Shutte, C.A., Joye, S.B., Hughes, A.H., Anderson, J.L.

2015. Groundwater controls ecological zonation of salt marsh macrophytes. *Ecology* **96**, 840–849

Wilson, A. M. & Gardner, L. R. 2006. Tidally driven groundwater flow and solute exchange in a marsh: Numerical simulations: TIDAL GROUNDWATER FLOW AND TRANSPORT. *Water Resour. Res.* **42**.

Wilson, A.M., Moore, W.S., Joye, S.B., Anderson, J.L., Schutte, C.A. 2010. Storm-driven groundwater flow in a salt marsh. *Water Resources Research* 47.

Xiao, K., Wilson, A.M., Li, H., Ryan, C. 2019. Crab burrows as preferential flow conduits for groundwater flow and transport in salt marshes: A modeling study. *Advances in Water Resources* 132.

APPENDIX A

AUXILIARY FIGURES

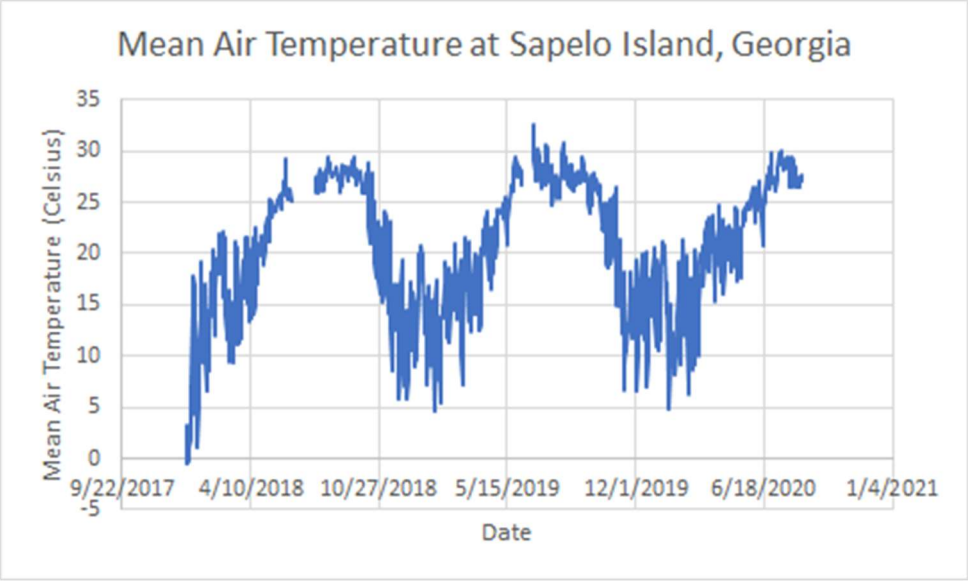

Figure A1. Mean air temperature at Sapelo Island, Georgia, 2018-2020.

Table A1. Palmer Drought Severity Index values for 2018-2020.

Month, Year	PDSI range	Drought Category
Jan-18	-1.99 to +1.99	Normal
Feb-18	-2.00 to -2.99	Moderate Drought
Mar-18	-2.00 to -2.99	Moderate Drought
Apr-18	-2.00 to -2.99	Moderate Drought
May-18	-1.99 to +1.99	Normal
Jun-18	-1.99 to +1.99	Normal
Jul-18	-1.99 to +1.99	Normal
Aug-18	-1.99 to +1.99	Normal
Sep-18	-1.99 to +1.99	Normal
Oct-18	-1.99 to +1.99	Normal
Nov-18	-1.99 to +1.99	Normal
Dec-18	+2.00 to +2.99	Moderately Moist
Jan-19	-1.99 to +1.99	Normal
Feb-19	-1.99 to +1.99	Normal
Mar-19	-1.99 to +1.99	Normal
Apr-19	-1.99 to +1.99	Normal
May-19	-2.00 to -2.99	Moderate Drought
Jun-19	-1.99 to +1.99	Normal
Jul-19	-2.00 to -2.99	Moderate Drought
Aug-19	-2.00 to -2.99	Moderate Drought
Sep-19	-3.00 to -3.99	Severe Drought
Oct-19	-3.00 to -3.99	Severe Drought
Nov-19	-2.00 to -2.99	Moderate Drought
Dec-19	-1.99 to +1.99	Normal
Jan-20	-1.99 to +1.99	Normal
Feb-20	-1.99 to +1.99	Normal
Mar-20	-1.99 to +1.99	Normal
Apr-20	-1.99 to +1.99	Normal
May-20	-1.99 to +1.99	Normal
Jun-20	-1.99 to +1.99	Normal
Jul-20	-1.99 to +1.99	Normal
Aug-20	-1.99 to +1.99	Normal
Sep-20	-1.99 to +1.99	Normal
Oct-20	-1.99 to +1.99	Normal
Nov-20	-1.99 to +1.99	Normal
Dec-20	-1.99 to +1.99	Normal
Jan-21	-1.99 to +1.99	Normal
Feb-21	-1.99 to +1.99	Normal
Mar-21	-1.99 to +1.99	Normal

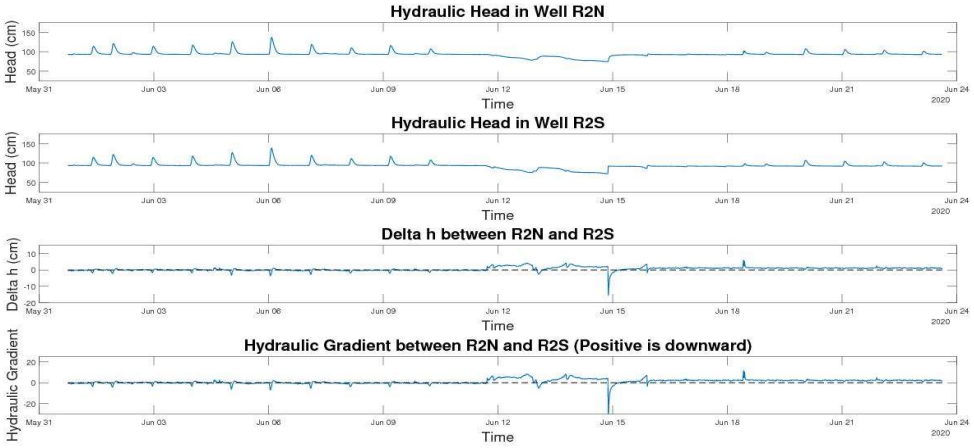

Figure A2. Vertical hydraulic gradient in wells R2A and R2B.

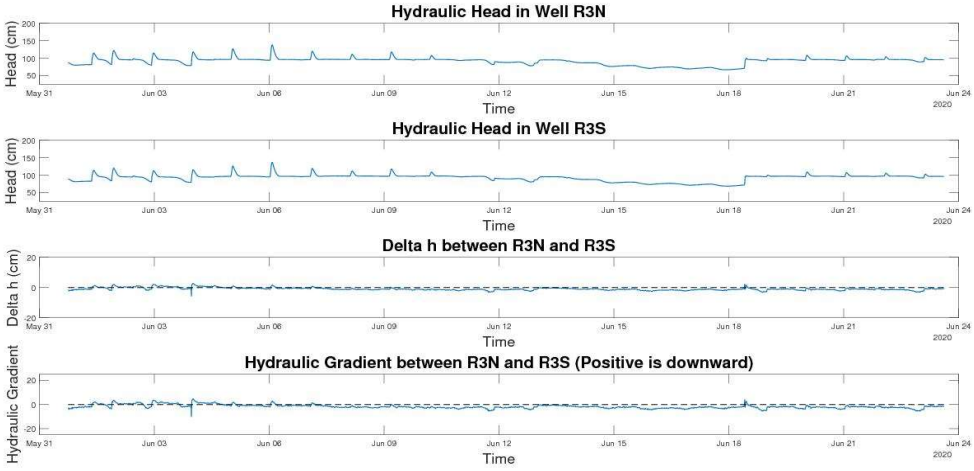

Figure A3. Vertical hydraulic gradient between wells R3A and R3B.

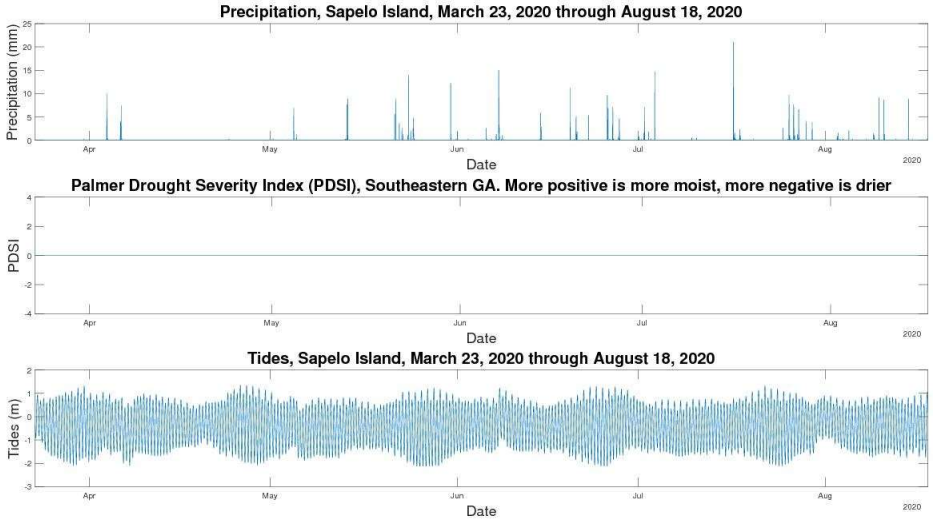

Figure A4. Tides and precipitation from late March through mid-August, 2020.

Table A2. Details about monitoring loggers installed at the Marsh Landing Wells.

Logger	Stick-up (cm)	Internal casing length (cm)
R2A	99.7	89.7
R2B	127.95	117.95
R3A	86.36	76.36
R3B	126.37	116.37
R4	127	117

Table A3. Goodness of fit of modeled hydraulic heads to observed hydraulic heads.

Well	R-Squared	Root Mean Square Error
R2A	0.06	12.98
R2B	0.07	15.08
R3A	0.56	8.14
R3B	0.58	9.22
R4	0.89	9.31
All Wells	0.5	11.26

APPENDIX B

MODEL BUILDING

Instructions for using modified SUTRA 2D3D with sc pre-processor:

1) Run sc.f to create mesh
    a) Put desired elevations in sc.dat
    b) Check sc.in, make sure that width matches x range in sc.dat, put desired nrow and ncol in, adjust hinit, density, gravity.
    c) Compile sc.f (**gfortran sc.f -o sc**)
    d) Run sc.f - should produce files sc.out, ics.out, sc2.out, DS14.txt, DS15b.txt, DS22.txt
    e) Paste ics.out into a correctly formatted <yourname>.ics.out (in my case, into AW.ics.out) - you have to do this because the ics.out produced by sc.f is missing the other data sets (you paste it into <yourfile>.ics.out data set 2- sc.f produces initial pressure conditions only)
    f) IF you **do not** have different sediment types, paste sc2.out into <yourfile>.inp. There are instructions about where to paste what.
        i) IF you **do** have different sediment types, paste ONLY DS3, DS17/19, DS22 into <yourfile>.inp (from sc2.out).
        ii) Sc.f produces DS14 and DS15 as text files also, yay! Inpolygon.m is a matlab code that assigns sediment parameters to the mesh by reading in DS14 and DS15, deciding if it is in a polygon of a certain sediment type, and assigns those sediment parameters to the mesh if the mesh occupies the same space as the sediment polygon. Its output looks like this:
            - The things you need to run this code are: the DS14, DS15, and DS22 text files, and a csv file for each of your desired sediment types with their coordinates
            - **The output of the inpolygon.m code is two csv files: "DS14new.csv" and "DS15new.csv" - copy and paste these into their respective data sets in <yourfile>.inp**

2) Create ytop and dx.dat files (inpolygon does this now!)
    a) Ytop.dat and dx.csv are outputs of inpolygoncode.mat (MAKE SURE YOU HAVE CORRECT NUMBER OF ROWS & COLUMNS IN LINE 18-20 OF THIS CODE)

b) Ytop.dat can be moved to the folder with the other SUTRA input files, no changes needed
    i) Ytop.dat should basically repeat the land surface elevation for every node in that column for every column. For example, if you have 5 nodes in each column and the first two land surface elevations are 1m and 2m you should have a column of 1m five times and a column to the right of it with 2m 5 times.
c) Copy the dx.csv into dx.dat, make sure to format it correctly.
    i) Dx.dat should be every node in DS17/19 and the width of the nodes, with the first and last value being half of the width since it is on the end. With precip in m/s, the dx.dat widths in m.
    ii) Dx.dat formatting:

        First row: number of columns
        Second row: -number of rows, half of your element width
        Third row-second to last row: -(top node), element width
        Last row: final node, half of element width

        Example: Model with 4 columns, 5 rows in each column, 6m apart each

        4
        -5 3
        -10 6
        -15 6
        -20 3

3) Creating newtide.in
    a) "Newtideinbuild.m" creates newtideinput.csv, which you can copy and paste into newtide.in for correct formatting.
    b) This code reads in tidal and precip data (I usually have to manually upload these parts) and interpolates the data into the correct time step size.

4) Running SUTRA - + input files
    a) Input files:
        i) Input files you have already made with above steps:
            (1) ytop.dat
            (2) dx.dat
            (3) <yourfile>.inp
            (4) <yourfile>.ics.out
        ii) Ones you need to prep

(1) **Tidal.param**: This file has pretty good instructions! Tide values are in m. Rainfall is m/s. Unsaturated flow parameters are: n, alpha, and residual saturation (in order) (see Carsel & Parrish, 1988 for estimates of these parameters)

(2) **Newtide.in** (if real tide): First line is the number of tide values to read in (in our case, one for each time step - so if 6000 time steps, you need 6000 newtide.in lines). The columns from left to right (tide(m), salinity (g/l), density (kg/m^3), precip (m/s), ET (m/s?)

(a) See "newtideinbuild.m" to build newtide.in

(3) <yourname>.inp: Observation nodes should reflect the wells you are modeling. Pick nodes close to them in elevation and distance from creek (DS 8D). Time steps also are adjusted here (DS 6). (Figure A2.2)

iii) Compile SUTRA: **gfortran *.f -o sutra -O3**

iv) Run SUTRA: produces .ele, .nod, .lst, .obs, .rst etc.

v) Run post processor - in cygwin "sh sh.post" (this converts .ele and .nod to .plt files for tecplot)

vi) Plot in tecplot: in cygwin "tecplot nod.plt" or "tecplot ele.plt"

5) Plotting heads with matlab

a) Prep <yourfile>.obs file

i) Open excel, copy and paste bottom part of .obs file into excel (the part with the obs node pressures, concentrations, and saturations)

ii) Trim upper part (you need to have the same column numbers all the way down) - then use text to columns to give data its own cell - keep trimming down till only data are left - save this file with your desired run name as a CSV

iii) Use headcalc.m or headplot2_realvsmodelled.m (preferred) to process

iv) Make sure that obsnodes=<filename> is set to the current file name (whatever file you imported in/read in)

v) Make sure that the well elevations are correct (as in same elevation as the obs node used to represent them)

vi) Run! Will produce a head plot. Make sure if you're using the realvsmodelled code that the real data lines up with your model timing.

vii) Save head plot under same name as the csv file used to create it - keep good notes about what was different about each run!

(1) Figure B.1 indicates equation used for calculating hydraulic head.

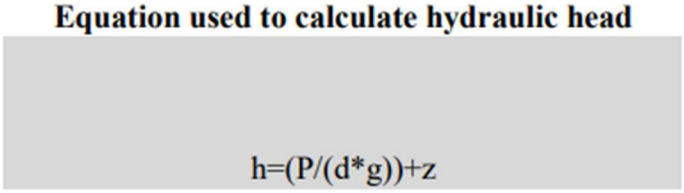

Figure B.1. Equation used to plot hydraulic head from model pressure outputs.

Table B.2. Model observation nodes selected to represent Marsh Landing wells.

Wells	Screen Depth (m)	x in cross section (m)	Land Surface Elevation (m)
R4	1.5	498.107	1.318
R3A	0.6	460.24	0.989
R3B	1.15	460.24	0.989
R2A	0.7	439.849	0.943
R2B	1.2	439.849	0.943
Elev of well (ideal) (m)	**Best fit observation node**	**Nodal elevation (m)**	**Difference between ideal and model (m)**
-0.182	7728	-0.229	0.047
0.389	7150	0.405	-0.016
-0.161	7146	-0.094	-0.067
0.243	6834	0.242	0.001
-0.257	6830	-0.262	0.005